

Evaluation of CHB MLI based shunt APF using low pass filter and self-tuning filter

Musa Yusup Lada¹, Mohd Amran Mohd Radzi², Jasronita Jasni², Hashim Hizam²,
Auzani Jidin¹, Syahrul Hisham Mohamad¹

¹Power Electronic and Drive Laboratory, Center for Robotics and Industrial Automation, Faculty of Electrical Engineering, Universiti Teknikal Malaysia Melaka (UTeM), Melaka, Malaysia

²Advanced Lightning, Power and Energy Research (ALPER) Centre, Faculty of Engineering, Universiti Putra Malaysia (UPM), Selangor, Malaysia

Article Info

Article history:

Received Apr 28, 2023

Revised May 10, 2023

Accepted May 23, 2023

Keywords:

Low pass filter

Multilevel inverter

Self-tuning filter

Shunt active power filter

Total harmonic distortion

ABSTRACT

The increasing demand for high-rating power supply in the distribution system causes the conventional inverter topology, six step voltage source inverter (SSVSI) unsuitable for being applied as active power filter (APF). Multilevel inverter (MLI) is generally the best suitable inverter for APF, but not all types of MLI can be used for high-voltage applications. Among the MLIs topology, cascaded H-bridge (CHB) is the best choice since it can produce output voltage more than twice the amount of DC source. Moreover, CHB MLI topology uses fewer power devices and is simple in design. Low pass filter (LPF) is a common method used for harmonic extraction in this controller. However, this method faces various problems, such as an additional need for phase lock loop (PLL) algorithm and slow transient and steady-state responses. Therefore, self-tuning filter (STF) is introduced as a new filtering method to overcome this problem. This paper evaluates CHB MLI's performance for APF using STF as a harmonic extraction. The model was developed and verified in MATLAB/Simulink. The results show that harmonic extraction using STF performs better total harmonic distortion (THD) than conventional LPF. Nevertheless, both algorithms produce THD below 5%, defined as the permissible value stated in IEEE 519.

This is an open access article under the [CC BY-SA](https://creativecommons.org/licenses/by-sa/4.0/) license.



Corresponding Author:

Musa Yusup Lada

Power Electronic and Drive Laboratory, Center for Robotics and Industrial Automation

Faculty of Electrical Engineering, Universiti Teknikal Malaysia Melaka (UTeM)

76100 Durian Tunggal, Melaka, Malaysia

Email: musayl@utem.edu.my

1. INTRODUCTION

Power quality is a general term used to represent the interaction of electrical power with electrical equipment. It is defined in the IEEE 100 authoritative dictionary of IEEE standard term as the concept of powering and grounding sensitive equipment in a manner that is suitable to the operation of that equipment. Since the late 1980s, power quality problem has become a priority in the distribution system. Three parties are concerned about power quality; utility companies, equipment manufacturers and electric power consumers. The characteristics of the power quality of the AC power system are divided into two, which are total harmonic distortion (THD) and power factor (PF) [1]. Besides, there are two power quality terms widely used in power systems. First, it is called good power quality, which can be used to define a power supply that is always available, consistently within the voltage and frequency tolerance. Then any load connected to it will run smoothly and efficiently. In addition, having a pure, noise-free sinusoidal wave shape is one of the characteristics of good power quality.

Meanwhile, poor power quality in a power system is defined when the load connected to it fails or has a reduced lifetime and efficiency of the electrical installation. Besides, poor power quality can affect the accuracy of utility metering. Moreover, the equipment in use is vulnerable to damage or service disturbance which will cause the maloperation of equipment and premature failure [2]–[4]. Harmonic distortion is caused by non-linear loads that are connected to the power system. Due to the increased non-linear loads used in daily life, it has gained endless attention. The voltage and current harmonics come from power electronic devices. They have been widely used in electrical components such as choppers, rectifiers and cyclo-converter. These non-linear loads affect the power flow by drawing currents only during certain intervals of the fundamental period. When the supplied current is not drawn linearly, as in a sinusoidal waveform, it will draw a higher percentage of harmonic distortion. Harmonic also can be observed when the current is not in a sinusoidal pattern, although the voltage supply is in the sine wave. Examples of non-linear loads that produce high harmonic distortion are transformers, arc furnaces, variable frequency drives and equipment like computers and copy machines [5], [6].

IEEE standard 519-2014, “IEEE Recommended Practice and Requirements for Harmonic Control in Electrical Power System” provides guidelines, limitations and procedures for applying harmonics limits in power systems. This standard is commonly applied to each type of static power converter used in industrial power systems. It briefly explains that the THD of the current drawn must be below 5%, and harmonic for a single component must not exceed 3%. IEEE 519-2014 will ensure that multiple customers consistently produce less amount of harmonic voltage. However, this standard is not covering the effect of radio frequency interference. In the power system, filtering is crucial to protect the consumer from an inadequate supply voltage quality. Usually, the non-linear loads generate harmonic current, distorting the voltage waveform. There are two types of harmonic elimination: passive power filter (PPF) and active power filter (APF). PPF is a simple filter that consists of four components made by the passive elements such as capacitance, inductance, damping resistor and transformer. PPF is a filter with no active component; thus, it does not need an additional power supply for its operation. In addition, previous studies state those PPFs not only filter current components but are also sources of reactive power that can be used for compensation [7], [8].

The increasing demand for high-rating power supply in the distribution system will cause the conventional inverter topology, the six-step voltage source inverter (SSVSI), becomes unsuitable for APF. In this case, multilevel inverter (MLI) is the most suitable inverter for APF, but not all types of MLI can be used for high-voltage applications. Cascaded H-bridge (CHB) topology is a better choice than other MLIs because it can produce output voltage more than twice the amount of DC source. Moreover, this topology uses fewer power devices and is simple in design. However, on the other hand, CHB topology faces a critical problem with a voltage unbalance of the DC-link capacitor, leading to bad performance in the compensation process and unequal stress of semiconductor devices. In addition, a more complicated problem occurs by maintaining the DC-link capacitor voltage if the CHB MLI produces more level of output voltage [9].

Therefore, this paper presents the evaluation performance of CHB MLI by using two different types of harmonic extraction, namely low pass filter (LPF) and self-tuning filter (STF) used in shunt APF (SAPF). Both harmonic extraction mechanisms will use the same switching algorithms and DC link capacitor algorithms, which are space vector pulse width modulation (SVPWM) and PI controller algorithms. Also, both harmonic extraction algorithms are tested under steady-state and dynamic-state conditions. Under steady-state conditions, the THD of the line current will be compared, and under dynamic-state conditions, the transient response will be compared.

2. PROPOSED METHOD

There are three main algorithms involved in the operation of APF: harmonic extraction, DC link capacitor, and switching algorithm. Each algorithm was designed and developed using MATLAB/Simulink tool. The harmonic extraction algorithm, also known as the current reference algorithm, intentionally produces the reference signal current (i_{ref}) used to generate the switching signal for the inverter. The DC link capacitor algorithm maintains voltage at the capacitor on a specific desired value to make the inverter work as APF, producing the current injected into the point of common coupling (PCC). Figure 1 shows the control algorithms using different harmonic extraction techniques: LPF and STF.

2.1. Multilevel inverter in SAPF

The MLI has been presented since 1975 as an alternative in producing medium and high voltage for several applications. The main purpose of MLI is to synthesize a near-sinusoidal voltage from several levels of DC voltages. As the number of levels increases, it will provide a staircase wave that approaches a desired waveform; hence the harmonic distortion of the output wave will be decreased. MLI comes in three types: diode clamped MLI, flying capacitors MLI and cascaded H-bridge MLI. Based on the current scenario of APF, most are using SSVSI, which is based on six switches and, at the same time, only capable of being used in low

and medium-voltage applications. Among MLI, only CHB can operate in high voltage applications due to its ability to produce output voltage twice the DC input. The advantages of CHB MLI in high voltage applications are transformerless, more economical, capable of producing a low harmonic output current, high efficiency for fundamental frequency, ability to work under high switching frequency and reduced voltage stresses across switches. In addition, the increasing number of H-bridges will synthesize the output waveform to add more steps in output voltage, producing a staircase wave to approach the sinusoidal wave with minimum harmonic distortion. Figure 2 shows the CHB MLI configuration in SAPF [10]–[15].

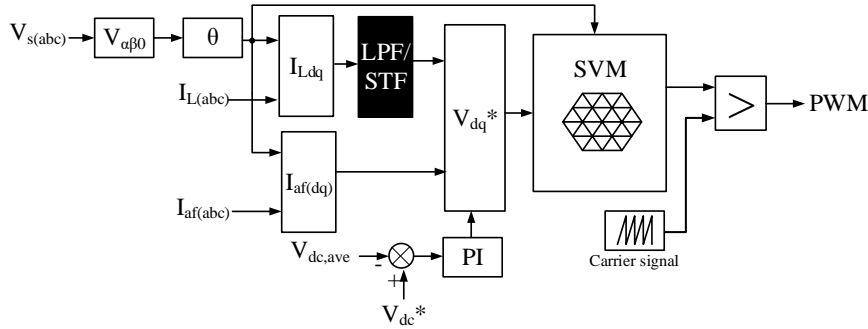


Figure 1. LPF and STF in SAPF

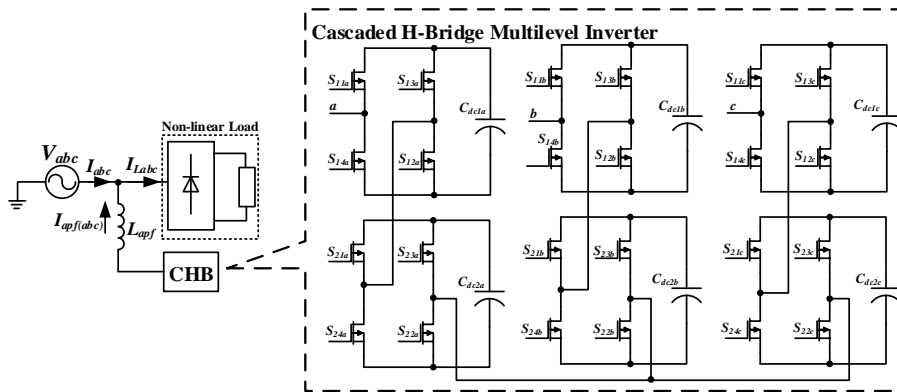


Figure 2. CHB MLI configuration in SAPF

2.2. Harmonic extraction

The conventional technique used in APF for harmonic extraction algorithms is LPF. The major drawback of using LPF is the high percentage error value produced in phase and magnitude of the harmonic components, which contribute to mitigating high-order harmonic components. Due to the drawback of LPF, a STF is introduced to overcome the time response issue in transient and steady-state conditions in the distribution power system. The advantages of the STF are working well in steady and transient state conditions, does not require phase lock loop (PLL), has no unity gain and phase delay at the fundamental frequency component and is easy to implement in a digital or analogue control system. The modification of the harmonic extraction from LPF to STF will significantly improve the performance of SAPF [16]–[22].

2.2.1 Low pass filter (LPF)

The capability of LPF is to allow lower frequencies below a selected cut-off frequency through the filter and block frequencies higher than the cut-off frequency. The Butterworth LPF is used in this research due to its advantages, such as a smooth passband and stopband, working capability in high order and the lowest dispersion characteristic. The transfer function of the generalized form of frequency response for n^{th} order Butterworth LPF shows in (1), where n is the order of the filter, ω is the passband frequency, ω_c is the cut-off frequency, and ε is the maximum passband gain. The quality factor, or the damping ratio for Butterworth LPF, is set to 0.707. The order of Butterworth LPF can be determined using the normalized Butterworth equation as stated in (2), in which the equation uses the real coefficients to be multiplied by the pole pair written in complex

conjugates. Moreover, in the second order of Butterworth LPF with the cut-off frequency of 50Hz and $\omega_c = 2\pi f_c$, the transfer function can be written as stated in (3).

$$H(s) = \frac{1}{\sqrt{1+\varepsilon^2\left(\frac{\omega}{\omega_c}\right)^{2n}}} \tag{1}$$

$$B_n(s) = \prod_{k=1}^{\frac{n}{2}} \left[s^2 - 2s \cos\left(\frac{2k+n-1}{2n}\pi\right) + 1 \right]; n = \text{even} \tag{2}$$

$$H_2(s) = \frac{1}{B_2(s)} = \frac{\omega^2}{s^2 - 1.414\zeta\omega s + \omega^2} \tag{3}$$

Bode plot frequency response of the Butterworth LPF is shown in Figure 3 with the order value of the n^{th} set from 1 to 10. Figure 3(a) represents the magnitude while Figure 3(b) illustrates the phase of Butterworth LPF. The cut-off frequency of the Butterworth LPF is 100π rad/s or equal to 50 Hz as the fundamental frequency of the supply. Thus, the harmonic component above the cut-off frequency will be mitigated. Therefore, only the harmonic component at the fundamental frequency component will remain. Based on (2) and (3), the increasing order value of n^{th} in Butterworth LPF will increase the complexity of the transfer function equation even though the shape of magnitude will approach the ideal characteristic of LPF. Thus, this will affect the time response due to the calculation process.

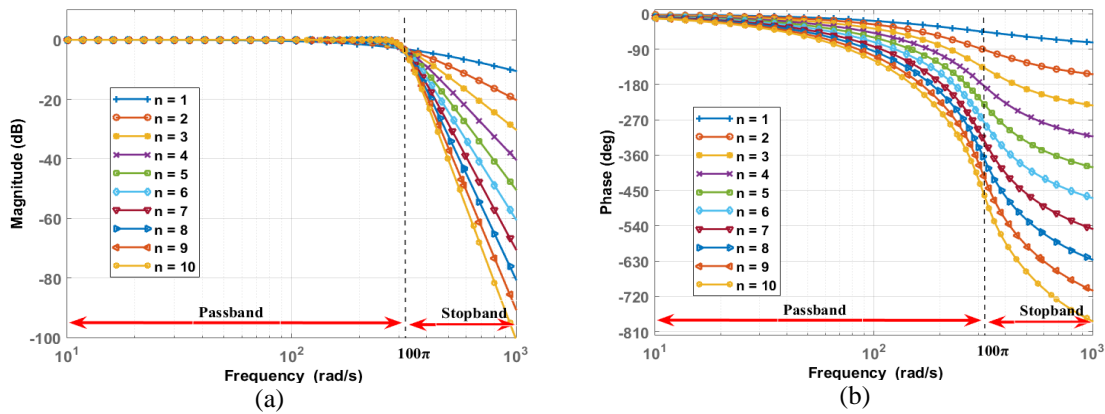


Figure 3. Frequency response of butterworth LPF in SAPF: (a) magnitude and (b) phase

2.2.2. Self-tuning filter (STF)

Similar to the function of LPF, STF is used to extract the fundamental component of load current in the d - q reference frame. Since the load current of d - q needs to be filtered, the equation of synchronous frame can be written as stated in (4). Where $\hat{I}_{dq}(t)$ and $I_{dq}(t)$ represent the instantaneous signals of output and input of the STF filter respectively.

$$\hat{I}_{dq}(t) = e^{j\omega t} \int e^{-j\omega t} I_{dq}(t) dt \tag{4}$$

By using the laplace transformation and adding the constant K , in (4) can be written as a transfer function stated in (5).

$$H(s) = \frac{\hat{I}_{dq}(s)}{I_{dq}(s)} = \frac{s+j\omega}{s^2+\omega^2} = K \frac{(s+K)+j\omega_c}{(s+K)^2+\omega_c^2} \tag{5}$$

Hence, the d - q reference current can be expressed as,

$$\begin{bmatrix} \hat{I}_d(s) \\ \hat{I}_q(s) \end{bmatrix} = \frac{K}{(s+K)^2+\omega_c^2} \begin{bmatrix} (s+K) & -\omega_c \\ \omega_c & (s+K) \end{bmatrix} \begin{bmatrix} I_d(s) \\ I_q(s) \end{bmatrix} \tag{6}$$

If $A = \begin{bmatrix} (s+K) & -\omega_c \\ \omega_c & (s+K) \end{bmatrix}$ then $|A| = (s+K)^2 + \omega_c^2$. Hence (6) can be simplified as (7).

$$\begin{bmatrix} (s + K) & \omega_c \\ \omega_c & (s + K) \end{bmatrix} \begin{bmatrix} \hat{I}_d(s) \\ \hat{I}_q(s) \end{bmatrix} = K \begin{bmatrix} I_d(s) \\ I_q(s) \end{bmatrix} \tag{7}$$

By separating $\hat{I}_d(s)$ and $\hat{I}_q(s)$ component in (7), the equation of $\hat{I}_d(s)$ and $\hat{I}_q(s)$ can be written as shown in (8) and (9). Whereby, $I_d(s)$ and $I_q(s)$ are the input signals meanwhile $\hat{I}_d(s)$ and $\hat{I}_q(s)$ are the output signals from the STF, which can be expressed in block diagram at Figure 4.

$$\hat{I}_d(s) = \frac{1}{s} (K[I_d(s) - \hat{I}_d(s)] - \omega_c \hat{I}_q(s)) \tag{8}$$

$$\hat{I}_q(s) = \frac{1}{s} (K[I_q(s) - \hat{I}_q(s)] - \omega_c \hat{I}_d(s)) \tag{9}$$

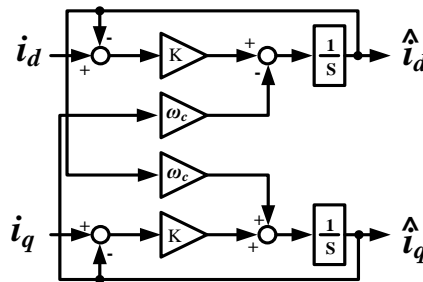


Figure 4. Block diagram of STF

The constant value K is also known as the selectivity parameter. Its value will affect the STF's performance, as shown in the Frequency response of the STF in SAPF in Figure 5. The magnitude and phase plots are illustrated in Figures 5(a) and 5(b) respectively, for a range of K from 20 to 100. Based on the magnitude and phase of the bode plot, the cut-off frequency of the STF is 100π rad/s or equal to 50 Hz as the fundamental frequency of the supply. Therefore, the harmonic component above the cut-off frequency will be mitigated, and only the fundamental component will remain. It is noticeable that the decrement of K in phase will make the shape of the frequency response approach the ideal characteristic of STF. By reducing the value of K , the fundamental component obtained from the distorted load current will not have phase delay and amplitude change. It is because the smaller value of K will increase the filter selectivity in STF.

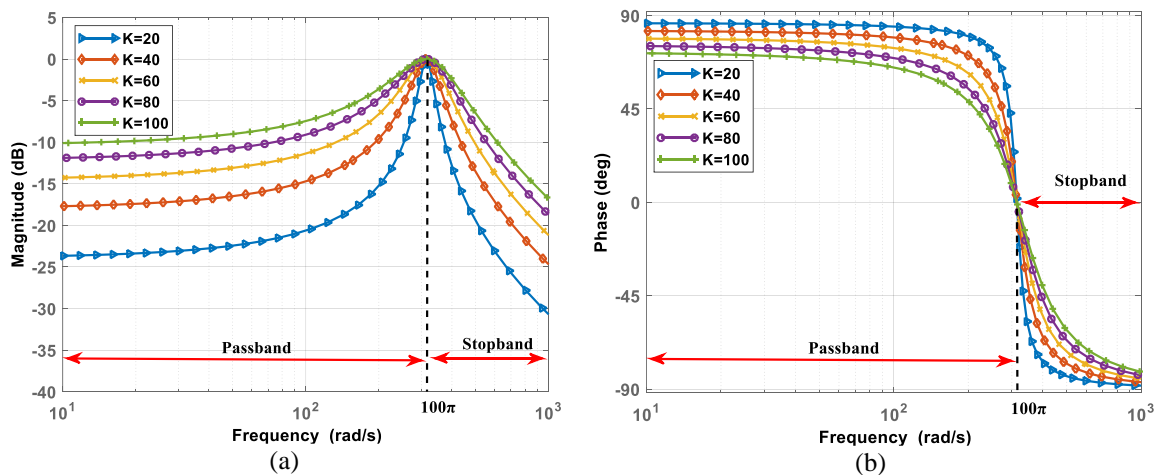


Figure 5. Frequency response of the STF in SAPF: (a) magnitude and (b) phase

2.3. DC link capacitor

A DC link capacitor, C_{dc} , is used as the storage element of the SAPF, which works continuously in a charged or discharged voltage condition from the power system to the load. The stability of SAPF depends on

the ability of voltage balancing algorithms to maintain the DC voltage at the DC link capacitor closer to the reference value of the capacitor voltage. If the voltage is below the reference value, SAPF cannot operate accordingly to mitigate the harmonics. The instantaneous reference energy of storage $W_{dc,ref}$ shown in (10) based on the instantaneous reference voltage drop across the DC link capacitor $V_{dc,ref}$. Therefore, the value of the DC link capacitor needs to be appropriately selected to effectively control the amplitude voltage fluctuations across the DC link capacitor.

$$W_{dc,ref}(t) = \frac{1}{2} C_{dc} V_{dc,ref}^2(t) \tag{10}$$

The change of instantaneous energy of the DC link capacitor within period one cycle shows in (10), in which the load current will charge and discharge the DC link capacitor at the steady state condition. Therefore, by using the energy balance concept, the charge of the capacitor energy is equal to the reactive and harmonic of the load current as stated in (11). By rearranging (11), the minimum size of the DC link capacitor can be written in (13), where ΔV_{dc} is the maximum or minimum DC bus capacitor voltages, $V_{dc,ref}$ is the DC bus capacitor voltage reference, V_s is the RMS value of source voltage, and ΔI_L is the peak RMS value of the reactive load current.

$$\Delta W_{dc}(t) = W_{dc,ref}(t) - W_{dc}(t) \tag{11}$$

$$\frac{1}{2} C_{dc} [\Delta V_{dc}^2 - \Delta V_{dc,ref}^2] = \frac{1}{2} \sqrt{2} V_s \Delta I_L \frac{T}{2} \tag{12}$$

$$C_{dc} \geq \frac{\sqrt{2} V_s \Delta I_L T}{2 [\Delta V_{dc}^2 - \Delta V_{dc,ref}^2]} \tag{13}$$

CHB MLI SAPF for a three-phase three-wire system uses six DC-link capacitors, controlled by a PI controller in each DC link capacitor connected to each H-Bridge inverter. Let K_p and K_i set to 0.8 and 8, respectively, so that voltage drops in each capacitor, either in the transient or steady-state conditions, can be controlled. By adding all DC link capacitors, $n = 6$, which is the total DC link capacitor voltage used in CHB MLI SAPF [23]–[29].

2.4. Space vector pulse width modulation (SVPWM)

SVPWM is generally popular because of several features, such as good utilization of DC link voltage and low current ripple. These features make SVPWM suitable for use in high voltage applications. However, this technique is quite complicated due to the process of formulating the sector, table requirements and the switching intervals for all vector positions. Despite this complexity, the designed algorithm is easy to apply in hardware implementation. SVPWM is well known as an alternative and popular control method for determining the switching pulse width and position. The fact that there is a degree of freedom of placement of the space vector in the switching cycle in SVPWM contributes to improving the harmonic performance in MLI. When compared to SPWM, SVPWM obtains a better voltage ratio value and can produce a greater maximum peak output voltage.

The SVPWM algorithm’s construction involves a space vector diagram and space voltage sector as depicted in Figure 6. Figure 6(a) shows the principle of SVPWM representing the three-phase output voltage of the inverter illustrated in the space vector diagram, which consists of six sectors and the resultant space voltage in the sector I. The detailed phasor diagram of the space voltage vector (\bar{v}) is shown in Figure 6(b). It can be written in (14), where t_z , t_a and t_b are the respective times for applying zero vector (\bar{v}_z), and two adjacent vectors (\bar{v}_a and \bar{v}_b). T is the sampling time for one cycle period which is equal to sum of t_z , t_a and t_b .

$$\bar{v} = \bar{v}_a \frac{t_a}{T} + \bar{v}_b \frac{t_b}{T} + \bar{v}_z \frac{t_z}{T} \tag{14}$$

The on duration for applying voltage vector \bar{v}_a , \bar{v}_b and \bar{v}_z at (14) can be obtain as:

$$t_b = \sqrt{3} \frac{v_q}{V_{dc}} T \tag{15}$$

where, $v_q = V \sin(\theta_{sec})$

$$t_a = \frac{3T}{2V_{dc}} \left(v_d - \frac{v_q}{\sqrt{3}} \right) \tag{16}$$

where, $v_d = V \cos(\theta_{sec})$
based on (15) and (16), Hence (17).

$$t_z = T - (t_a + t_b) \tag{17}$$

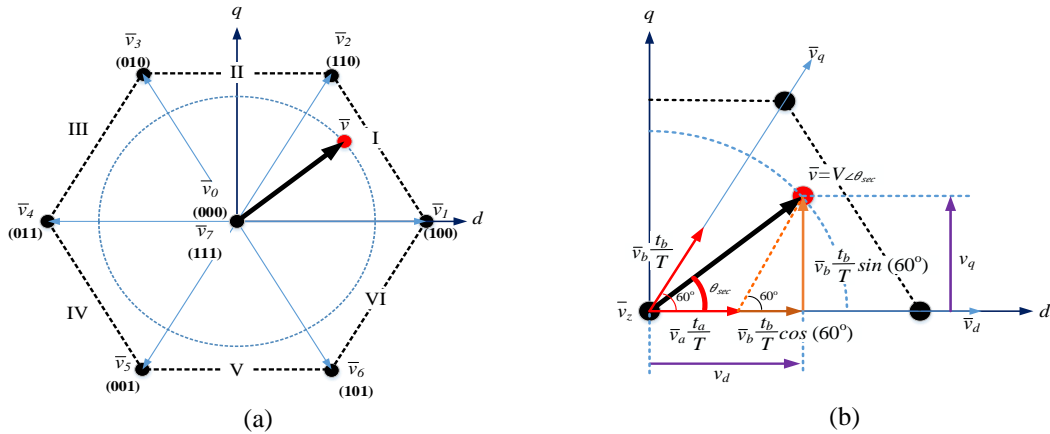


Figure 6. SVPWM algorithms (a) principle of SVPWM (b) resultant space voltage vector

3. RESULTS AND DISCUSSION

The LPF and STF harmonic extraction algorithms for CHB MLI are designed, developed and verified through MATLAB/Simulink tools using parameters stated in Table 1. The model of block control algorithms for LPF and STF are shown in Figure 7. Figure 7(a) depicts Simulink model for LPF harmonic extraction method, and Figure 7(b) is for Simulink model of STF technique. The self-tuning filter block in Figure 7(b) is constructed based on the proposed algorithm block diagram illustrated in Figure 4. In this experiment, the voltage supply uses a balanced sinusoidal voltage source with a different angle of 120°.

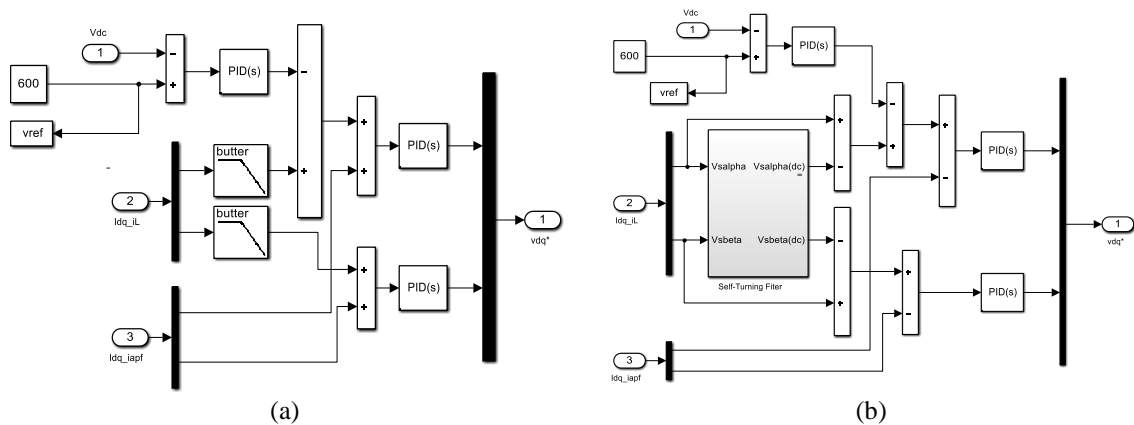


Figure 7. Block control algorithms for LPF and STF (a) simulation model of LPF based harmonic extraction and (b) Simulink model of STF based harmonic extraction

Table 1. Parameters of SAPF

Parameter	Value
Voltage source	400 Vrms 50 Hz
Smoothing inductor, I_{apf}	5 mH
Capacitor Link, C_{dc}	3300 μ F 400V (each)
Line inductor, I_l	2 mH
Switching frequency	20 kHz
Resistive load	Rectifier + 20 Ω
Inductive load	Rectifier + 50 mH (Series with 20 Ω)
Capacitive load	Rectifier + 100 μ F (Parallel with 20 Ω)

Figure 8 describes the results obtained using the LPF-based harmonic extraction method for inductive load at filter order n equal to 3. Figure 8(a) depicts three-phase line voltage, three-phase line current, three-phase load current and three-phase APF current. Figure 8(b) shows the voltage and current at Phase A, Figure 8(c) is the THD of the line current at Phase A and Figure 8(d) is the THD of the load current at Phase A.

In addition, Figure 9 illustrates the results of harmonic extraction for inductive load when the filter order increases at n equal to 9. Figure 9(a) represents three-phase line voltage, three-phase line current, three-phase load current and three-phase APF current. Figure 9(b) is the voltage and current at Phase A, Figure 9(c) displays the THD of the line current at Phase A and Figure 9(d) is the THD of the load current at Phase A. Based on the results, THD for $n = 3$ reduces from 29.36% (load current) to 1.15% (line current). Meanwhile, for $n = 9$, the THD drops from 29.36% (line current) to 1.13% (line current). The highest number of n will perform better mitigation of harmonics due to load current.

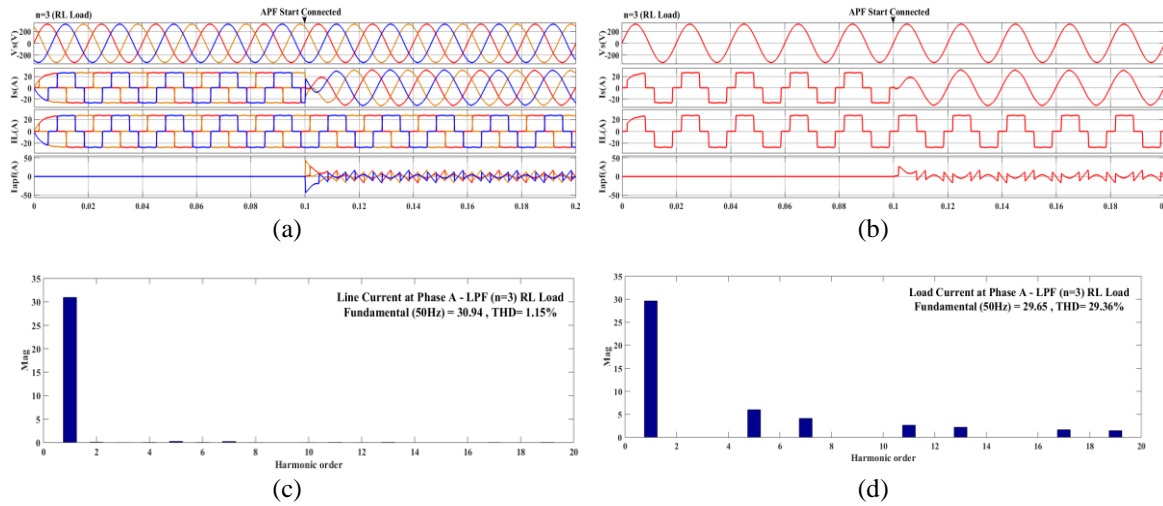


Figure 8. LPF based harmonic extraction for inductive load at $n=3$: (a) three-phase line voltage, three-phase line current, three-phase load current and three-phase APF current, (b) voltage and current at Phase A, (c) THD of line current at Phase A, and (d) THD of load current at Phase A

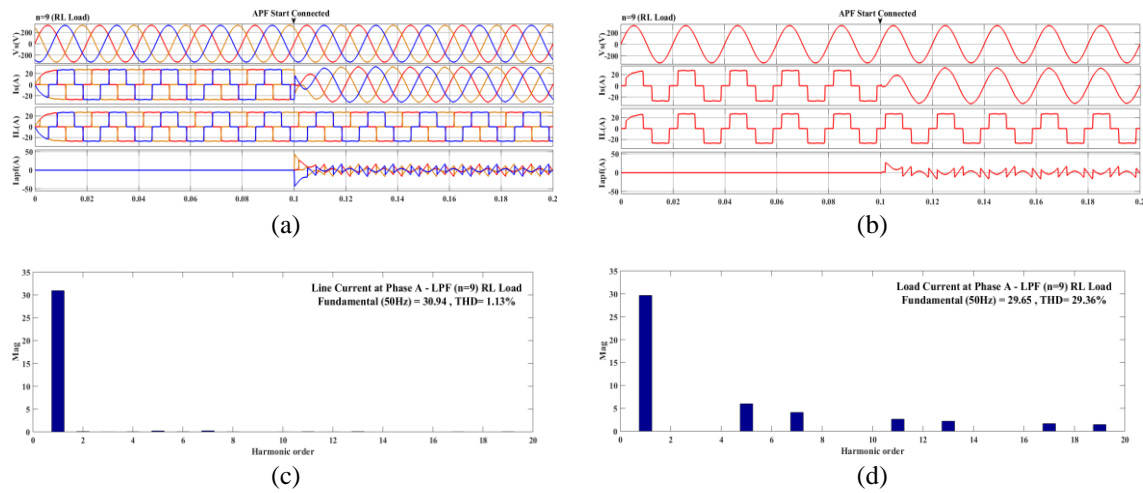


Figure 9. LPF based harmonic extraction for inductive load at $n = 9$: (a) three-phase line voltage, three-phase line current, three-phase load current and three-phase APF current, (b) voltage and current at Phase A, (c) THD of line current at Phase A, and (d) THD of load current at Phase A

Figure 10 shows the results obtained using the STF-based harmonic extraction method for inductive load at selective parameter K equal to 40. Figure 10(a) displays the three-phase line voltage, three-phase line current, three-phase load current and three-phase APF current. Figure 10(b) is the voltage and current at Phase A, Figure 10(c) shows the THD of line current at Phase A and Figure 10(d) is the THD of load current at Phase A. The results for the STF harmonic extraction method for inductive load when the selective parameter K equal to 100 are depicted in Figure 11. The arrangement and label for Figures 11(a)-11(d) follow the explanation as table in Figure 10. Based on the results, the THD for $K=40$ reduces from 29.36% (load current) to 0.96% (line

current). Meanwhile, for $K=100$ the THD drops from 29.36% (load current) to 1.50% (line current). The lowest number of K performs better harmonics mitigation due to the load current.

In addition, LPF and STF-based harmonic extraction methods are tested with several loads, with different numbers of n for LPF and K for STF. Both algorithms' performances are summarised and tabulated in Tables 2 and 3, respectively. From Table 2, the increased value of n in LPF produces a better percentage of THD of line current for all tested loads. Whereas, in Table 3, the decreased value of K in STF produces a better percentage of THD of line current for all tested loads. Both algorithms can mitigate more than 85% of the THD of load current. However, the LPF technique requires a higher order of n to produce less THD value. It is because the higher order will produce a frequency response approaching the ideal frequency response of LPF as shown earlier in Figure 3. In other words, the effect of higher order will shift the roll-off frequency response near to the ideal shape of LPF with the angle perpendicular to 90° . This high order of n requirement causes disadvantages when using the LPF method. It will make the equation more complex, contributing to the increment of calculation time in the processor.

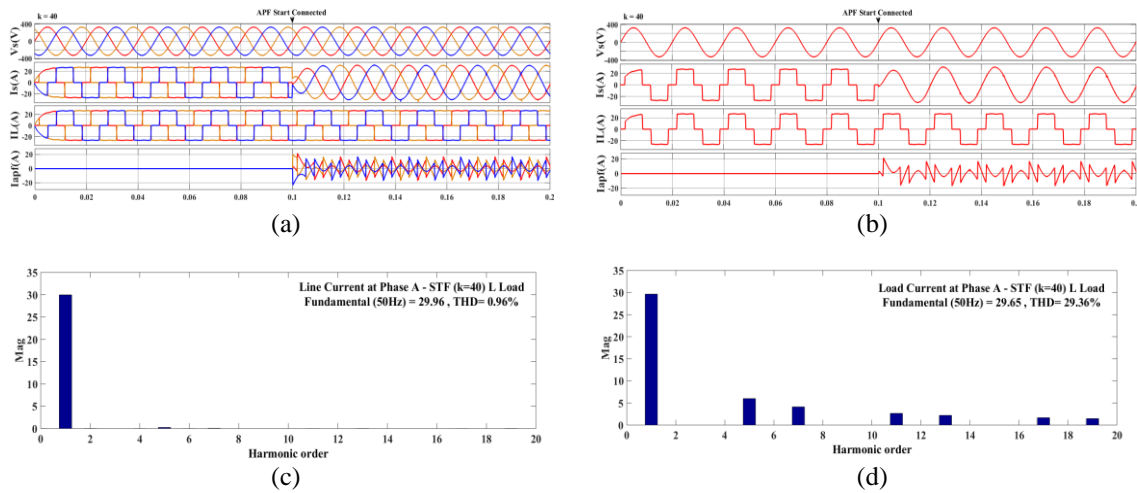


Figure 10. STF based harmonic extraction for inductive load at $K=40$: (a) three-phase line voltage, three-phase line current, three-phase load current and three-phase APF current, (b) voltage and current at Phase A, (c) THD of line current at Phase A, and (d) THD of load current at Phase A

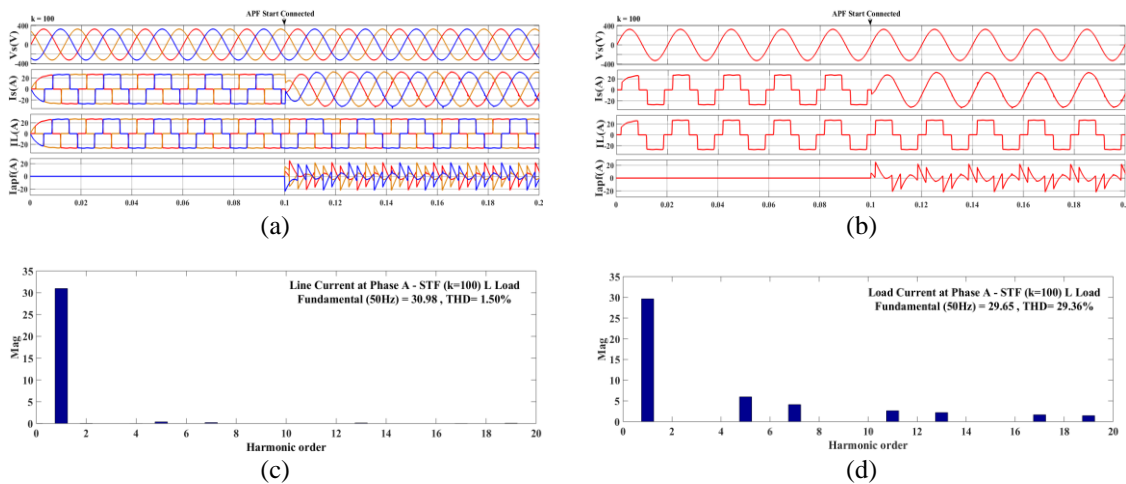


Figure 11. STF harmonic extraction for Inductive load at $K=100$: (a) three-phase line voltage, three-phase line current, three-phase load current and three-phase APF current, (b) voltage and current at Phase A, (c) THD of line current at Phase A, and (d) THD of load current at Phase A

Figure 12 shows the percentage reduction of THD of line current for both LPF and STF algorithms. As for STF algorithms, the decreasing value of K will affect the low value of the THD line current. Contradictory to LPF algorithms, the increasing value of n will affect the low value of the THD line current. According to the

graph pattern, the n value above three will reach a stable value of the THD line current. Meanwhile, for K value below 40 will reach a stable value of THD line current. The inductive load can produce the lowest THD line current for both algorithms due to the capability of inductive that can act as a current filter in the load.

Table 2. Performance of LPF with several loads

Load	LPF (THD of line and load current)														
	n = 1			n = 3			n = 5			n = 7			n = 9		
	Load (%)	Line (%)	$\Delta\%$	Load (%)	Line (%)	$\Delta\%$	Load (%)	Line (%)	$\Delta\%$	Load (%)	Line (%)	$\Delta\%$	Load (%)	Line (%)	$\Delta\%$
Resistive	29.47	3.98	86.5	29.47	1.53	94.8	29.47	1.50	94.9	29.47	1.50	94.9	29.47	1.50	94.9
Inductive	29.36	4.07	86.1	29.36	1.15	96.1	29.36	1.14	96.1	29.36	1.13	96.2	29.36	1.13	96.2
Capacitive	55.01	4.37	92.1	55.01	3.11	94.3	55.01	3.05	94.5	55.01	3.05	94.5	55.01	3.05	94.5

Table 3. Performance of STF with several loads

Load	STF algorithm technique (THD of line and load current)														
	K = 20			K = 40			K = 60			K = 80			K = 100		
	Load (%)	Line (%)	$\Delta\%$	Load (%)	Line (%)	$\Delta\%$	Load (%)	Line (%)	$\Delta\%$	Load (%)	Line (%)	$\Delta\%$	Load (%)	Line (%)	$\Delta\%$
Resistive	29.47	1.34	95.5	29.47	1.36	95.4	29.47	1.45	95.1	29.47	1.58	94.6	29.47	1.75	94.1
Inductive	29.36	0.93	96.8	29.36	0.96	96.7	29.36	1.09	96.3	29.36	1.29	95.6	29.36	1.5	94.9
Capacitive	32.51	1.59	95.1	32.51	1.72	94.7	32.51	1.87	94.2	32.51	2.05	93.7	32.51	2.25	93.1

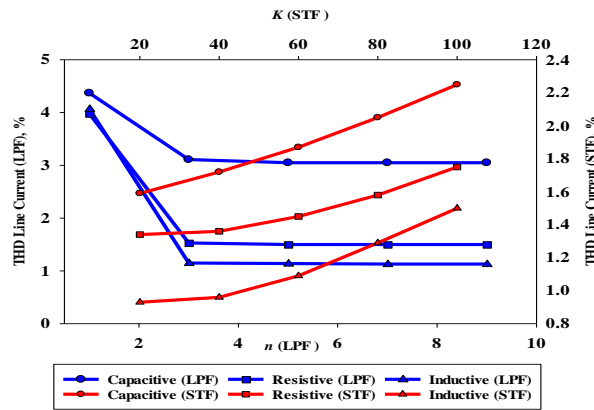


Figure 12. Percentage reduction of THD of current for LPF and STF algorithms

4. CONCLUSION

This paper demonstrates the performances of LPF and STF-based harmonic extraction algorithms in CHB MLI SAPF. The filter's order in LPF-based harmonic extractions needs to be increased to obtain a better percentage of THD of line current. Meanwhile, the value of the selective parameter needs to be decreased in STF-based harmonic extraction to achieve a lower percentage of THD of line current. Based on the simulation results, both harmonic extractions have successfully operated CHB MLI SAPF with THD to be below 5%, following the IEEE 519 Standard. In addition, STF-based harmonic extraction can mitigate more THD in load current compared to LPF-based harmonic extraction. However, to achieve the same performance as STF, the LPF needs to perform with high-order complex mathematical equations that contribute to creating time delay and, at the same time, decreasing the performance of SAPF. Furthermore, implementing high-order LPF-based harmonic extraction in hardware development is even more difficult.

ACKNOWLEDGEMENTS




This work was funded by Center for Research and Innovation (CRIM), Universiti Teknikal Malaysia Melaka (UTeM), under the PJP Grant (PJP/2022/FKE/S01856), in part by the Ministry of Higher Education (MOHE) and advanced lightning, power and energy research (ALPER) Centre, Universiti Putra Malaysia under PUTRA Grant (9656100).

REFERENCES




[1] L. Li, M. Hui, X. Xu, X. Chen, B. Sun, and Y. Xie, "Repetitive control implementation with frequency adaptive algorithm for shunt active power filter," in *2016 IEEE 8th International Power Electronics and Motion Control Conference, IPEMC-ECCE Asia 2016*, May 2016, pp. 1328–1332, doi: 10.1109/IPEMC.2016.7512482.

- [2] A. A. S. Mohamed, A. Berzoy, and O. A. Mohammed, "Adaptive transversal digital filter for reference current detection in shunt active power filter," in *IEEE Power and Energy Society General Meeting*, Jul. 2015, vol. 2015-Sept, doi: 10.1109/PESGM.2015.7286555.
- [3] L. B. G. Campanhol, S. A. O. da Silva, and A. Goedtel, "Application of shunt active power filter for harmonic reduction and reactive power compensation in three-phase four-wire systems," *IET Power Electronics*, vol. 7, no. 11, pp. 2825–2836, Nov. 2014, doi: 10.1049/iet-pel.2014.0027.
- [4] A. Teke, L. Saribulut, and M. Tumay, "A novel reference signal generation method for power-quality improvement of unified power-quality conditioner," *IEEE Transactions on Power Delivery*, vol. 26, no. 4, pp. 2205–2214, Oct. 2011, doi: 10.1109/TPWRD.2011.2141154.
- [5] Y. Hoon, M. A. M. Radzi, M. K. Hassan, and N. F. Mailah, "A simple neutral-point voltage deviation minimization method for three-level inverter-based shunt active power filter," *International Journal of Simulation: Systems, Science and Technology*, vol. 17, no. 41, pp. 33.1–33.6, Jan. 2017, doi: 10.5013/IJSSST.a.17.41.33.
- [6] Y. Hoon, M. A. M. Radzi, M. K. Hassan, and N. F. Mailah, "Neutral-point voltage deviation control for three-level inverter-based shunt active power filter with fuzzy-based dwell time allocation," *IET Power Electronics*, vol. 10, no. 4, 2017, doi: 10.1049/iet-pel.2016.0240.
- [7] M. Büyük, A. Tan, M. Inci, and M. Tümay, "A notch filter based active damping of LCL filter in shunt active power filter," in *19th International Symposium on Power Electronics, Ee 2017*, Oct. 2017, vol. 2017-Decem, pp. 1–5, doi: 10.1109/PEE.2017.8171701.
- [8] J. Morales, L. G. De Vicuna, R. Guzman, M. Castilla, and J. Miret, "Modeling and sliding mode control for three-phase active power filters using the vector operation technique," *IEEE Transactions on Industrial Electronics*, vol. 65, no. 9, pp. 6828–6838, Sep. 2018, doi: 10.1109/TIE.2018.2795528.
- [9] A. Panchbhai, N. Prajapati, and S. Parmar, "Comparative study of reference current generation for shunt active power filter," in *International Conference on Power and Embedded Drive Control, ICPEDC 2017*, Mar. 2017, pp. 381–386, doi: 10.1109/ICPEDC.2017.8081119.
- [10] A. Mortezaei, C. Lute, M. G. Simões, F. P. Marafão, and A. Boglia, "PQ, DQ and CPT control methods for shunt active compensators - A comparative study," *IEEE Energy Conversion Congress and Exposition, ECCE*, 2014, pp. 2994–3001, doi: 10.1109/ECCE.2014.6953807.
- [11] J. Chen, Z. Yin, P. Wang, and Y. Li, "Capacitor voltage balancing control of cascaded multilevel inverter for high-power active power filters," in *3rd International Conference on Deregulation and Restructuring and Power Technologies, DRPT 2008*, Apr. 2008, pp. 1683–1687, doi: 10.1109/DRPT.2008.4523676.
- [12] N. S. Rao, "Cascaded multilevel inverter based dstatcom for power line conditioners using instantaneous real-power theory," *International Journal of Electrical and Electronics Engineering Research (IJEEER)*, vol. 3, no. 4, pp. 1–14, 2013.
- [13] P. Karuppanan and K. Mahapatra, "A novel SRF based cascaded multilevel active filter for power line conditioners," Dec. 2010, doi: 10.1109/INDCON.2010.5712667.
- [14] W. Madhukar and P. Agarwal, "Comparison of control strategies for multilevel inverter based active power filter used in high voltage systems," Dec. 2010, doi: 10.1109/PEDES.2010.5712440.
- [15] S. Ray, N. Gupta, and R. A. Gupta, "Comparative analysis of conventional and modified peak-detection based control technique for cascaded H-bridge multilevel inverter based shunt active power filter," in *2017 Innovations in Power and Advanced Computing Technologies, i-PACT 2017*, Apr. 2017, vol. 2017-Janua, pp. 1–6, doi: 10.1109/IPACT.2017.8244898.
- [16] Y. Hoon, M. A. Mohd Radzi, M. K. Hassan, and N. F. Mailah, "Enhanced instantaneous power theory with average algorithm for indirect current controlled three-level inverter-based shunt active power filter under dynamic state conditions," *Mathematical Problems in Engineering*, vol. 2016, pp. 1–12, 2016, doi: 10.1155/2016/9682512.
- [17] Y. Hoon, M. A. M. Radzi, M. K. Hassan, and N. F. Mailah, "A refined self-tuning filter-based instantaneous power theory algorithm for indirect current controlled three-level inverter-based shunt active power filters under non-sinusoidal source voltage conditions," *Energies*, vol. 10, no. 3, p. 277, Feb. 2017, doi: 10.3390/en10030277.
- [18] Y. Hoon, M. A. M. Radzi, M. K. Hassan, and N. F. Mailah, "DC-link capacitor voltage regulation for three-phase three-level inverter-based shunt active power filter with inverted error deviation control," *Energies*, vol. 9, no. 7, p. 533, Jul. 2016, doi: 10.3390/en9070533.
- [19] Y. Hoon, M. A. M. Radzi, M. K. Hassan, N. F. Mailah, and N. I. A. Wahab, "A simplified synchronous reference frame for indirect current controlled three-level inverter-based shunt active power filters," *Journal of Power Electronics*, vol. 16, no. 5, pp. 1964–1980, Sep. 2016, doi: 10.6113/JPE.2016.16.5.1964.
- [20] Y. Hoon, M. A. M. Radzi, M. K. Hassan, and N. F. Mailah, "A self-tuning filter-based adaptive linear neuron approach for operation of three-level inverter-based shunt active power filters under non-ideal source voltage conditions," *Energies*, vol. 10, no. 5, p. 667, May 2017, doi: 10.3390/en10050667.
- [21] L. S. Stanly, R. Divya, and M. G. Nair, "Grid connected solar photovoltaic system with shunt active filtering capability under transient load conditions," in *Proceedings of IEEE International Conference on Technological Advancements in Power and Energy, TAP Energy 2015*, Jun. 2015, pp. 345–350, doi: 10.1109/TAPENERGY.2015.7229643.
- [22] Y. Han, P. Shen, and J. M. Guerrero, "Stationary frame current control evaluations for three-phase grid-connected inverters with PVR-based active damped LCL filters," *Journal of Power Electronics*, vol. 16, no. 1, pp. 297–309, Jan. 2016, doi: 10.6113/JPE.2016.16.1.297.
- [23] N. F. A. Rahman, M. A. M. Radzi, A. C. Soh, N. Mariun, and N. A. Rahim, "Significant insights into the operation of DC-link voltage control of a shunt active power filter using different control algorithms: A comparative study," *Turkish Journal of Electrical Engineering and Computer Sciences*, vol. 25, no. 3, pp. 2033–2043, 2017, doi: 10.3906/elk-1504-17.
- [24] N. F. A. Rahman, M. A. M. Radzi, A. C. Soh, N. Mariun, and N. A. Rahim, "Adaptive hybrid fuzzy-proportional plus crisp-integral current control algorithm for shunt active power filter operation," *Energies*, vol. 9, no. 9, p. 737, Sep. 2016, doi: 10.3390/en9090737.
- [25] S. Sreelakshmi, M. S. Sujatha, J. R. Rahul, and T. Sutikno, "Reduced switched seven level multilevel inverter by modified carrier for high voltage industrial applications," *International Journal of Power Electronics and Drive Systems (IJPEDS)*, vol. 14, no. 2, pp. 872–881, Jun. 2023, doi: 10.11591/ijpeds.v14.i2.pp872-881.
- [26] O. Y. K. Al-Atbee and K. M. Abdulhassan, "A cascade multi-level inverter topology with reduced switches and higher efficiency," *Bulletin of Electrical Engineering and Informatics*, vol. 12, no. 2, pp. 668–676, Apr. 2023, doi: 10.11591/eei.v12i2.4138.
- [27] M. T. Yaqoob, M. K. Rahmat, S. M. M. Maharum, and M. M. Su'ud, "A Review on harmonics elimination in real time for cascaded H-bridge multilevel inverter using particle swarm optimization," *International Journal of Power Electronics and Drive Systems (IJPEDS)*, vol. 12, no. 1, p. 228, Mar. 2021, doi: 10.11591/ijpeds.v12.i1.pp228-240.
- [28] M. A. Hutabarat, S. Hasan, A. H. Rambe, and S. Suherman, "Design and simulation hybrid filter for 17 level multilevel inverter," *Bulletin of Electrical Engineering and Informatics*, vol. 9, no. 3, pp. 886–897, Jun. 2020, doi: 10.11591/eei.v9i3.890.
- [29] M. Y. Lada, M. A. M. Radzi, J. Jasni, H. Hizam, A. Jidin, and S. H. Mohamad, "Performance of three-phase three-wire cascaded H-bridge multilevel inverter-based shunt active power filter," *International Journal of Power Electronics and Drive Systems (IJPEDS)*, vol. 11, no. 3, pp. 1430–1440, Sep. 2020, doi: 10.11591/ijpeds.v11.i3.pp1430-1440.




BIOGRAPHIES OF AUTHORS

Musa Yusup Lada    was born in Sabah, Malaysia, in 1984. He received his B.Eng. degree and M.sc. in Power Electronics and Drive from the Universiti Teknikal Malaysia Melaka (UTeM) in 2008 and 2013, respectively. He is presently working towards his Ph.D. degree in Electrical Power Engineering in the Department of Electrical and Electronic Engineering, Faculty of Engineering, Universiti Putra Malaysia. His current research interests include power electronics converter, power quality, and renewable energy. He can be contacted at email: musayl@utem.edu.my.






Mohd Amran Mohd Radzi    was born in Kuala Lumpur, Malaysia, in 1978. He received his B.Eng. (Hons.) degree in Electrical and Electronics Engineering and his M.S. degree in Electrical Power Engineering from the Universiti Putra Malaysia (UPM), Serdang, Selangor, Malaysia, in 2000 and 2002, respectively; and his Ph.D. degree in Power Electronics from the University of Malaya (UM), Kuala Lumpur, Malaysia, in 2010. He is presently working as a Professor in the Department of Electrical and Electronic Engineering, Faculty of Engineering, Universiti Putra Malaysia. His current research interests include power electronics, power quality, and renewable energy. He can be contacted at email: amranmr@upm.edu.my.






Jasronita Jasni    received B. Eng degree in Electrical Engineering (1998) and M. Eng. in Electrical Engineering (2001) from Universiti Teknologi Malaysia. She received the Ph.D. degree in Electrical Power Engineering from Universiti Putra Malaysia in 2010. Currently she is an Associate Professor in the Department of Electrical and Electronic Engineering, Universiti Putra Malaysia, Malaysia. She is an IEEE member. Her research interests include power system analysis for static and dynamics, load flow analysis, embedded generation and renewable energy. She can be contacted at email: jas@upm.edu.my.






Hashim Hizam    graduated with a B.Sc. and M.Sc. in Electrical and Electronic Engineering from Polytechnic University, Brooklyn, New York in 1993 and 1994, respectively. In 2004, he obtained his Ph.D. from Queen University Belfast, Northern Ireland in the UK. He is now an Associate Professor at the Department of Electrical and Electronic Engineering, Faculty of Engineering, Universiti Putra Malaysia. His areas of research are in power system protection and power system analysis. He also a member of the IEEE. He can be contacted at email: hhizam@upm.edu.my.



Auzani Jidin    received the B.Eng., M.Eng. and Ph.D. degrees in power electronics and drives from Universiti Teknologi Malaysia (UTM), Malaysia, in 2002, 2004, and 2011, respectively. He is currently a Senior Lecturer with the Department of Power Electronics and Drives, Faculty of Electrical Engineering, Universiti Teknikal Malaysia Melaka (UTeM), Malaysia. His research interests include the field of power electronics, motor drive systems, FPGA, and DSP applications. He can be contacted at email: auzani@utem.edu.my



Syahrul Hisham Mohamad    received his Bachelor Degree in Electrical and Electronics Engineering from Universiti Tenaga Nasional (UNITEN) in 2003 and Master of Engineering from Universiti Teknologi Malaysia (UTM) in 2013. He is currently working towards his Ph.D. degree in Electrical Power Engineering in the Department of Electrical and Electronic Engineering, Faculty of Engineering, Universiti Putra Malaysia. His current research interests include power electronics converter, power quality, and artificial intelligent. He can be contacted at email: syahrulhisham@utem.edu.my.